Deorbiting Dynamics of Electrodynamic Tether

Article · January 2011

DOI: 10.3850/2010428611000043

2 authors:

Z. H. Zhu
York University
115 PUBLICATIONS **637** CITATIONS
SEE PROFILE

Rui Zhong
Beihang University (BUAA)
19 PUBLICATIONS **93** CITATIONS
SEE PROFILE

International Journal of Aerospace and Lightweight Structures
Vol. 1, No. 1 (2011) 47–66

DOI: 10.3850/S2010428611000043

DEORBITING DYNAMICS OF ELECTRODYNAMIC TETHER

Z. H. ZHU* and RUI ZHONG†

Department of Earth and Space Science and Engineering
York University 4700 Keele Street, Toronto
Ontario M3J 1P3, Canada
**gzhu@yorku.ca*
†*rzhong@yorku.ca*

Accepted 28 August 2011

This paper studies satellite deorbit using electrodynamic tether (EDT) propulsion. Gaussian perturbation equations are used to model the orbital dynamics of EDT with environmental perturbations of electrodynamic force, aerodynamic drag and the effect of Earth's oblateness. Differential equations for the induced voltage-current across EDT are derived and solved with boundary conditions determined by mission objectives and hardware devices. A simplified analytical method for solving the equations is proposed to improve computational efficiency. Simulations find that the orbit of a satellite deorbited by EDT will become elliptical in near polar orbits due to the higher-order perturbation of Earth's magnetic field. This is beneficial for the near polar orbits where the electrodynamic force is less effective, because the atmosphere at a lower perigee will provide larger air drag to dissipate the orbital kinetic energy of satellite faster. Moreover, we proved that the polarity reverse of the induced voltage/current across EDT in near polar orbits does not affect the kinetic energy dissipation by the current induced Lorentz force. Compared the decay by air drag only, the orbit decaying time of a satellite with EDT will be reduced by three and two orders of magnitudes in the equatorial and polar orbits respectively.

Keywords: Electrtodynamic tether; deorbit; dynamics; tethered satellite; magnetic field.

1. Introduction

The concept of tethered satellite systems (TSS) has shown great potential in areas of long-baseline interferometer [Bombardelli *et al.*, 2004], power generation [Wen *et al.*, 2008], formation flying [Kumar, 2006], and space transportation [Cartmell and McKenzie, 2008]. Over the past four decades, TSS has been well-studied, and its feasibility is further demonstrated by several missions (e.g. TSS-1R [Sanmartin,

*Corresponding author.

2010], SEDS [Carroll, 1993], YES2 [Kruijff *et al.*, 2009], MAST [Hoyt *et al.*, 2003] and T-Rex [Fujii, 2010]). Strikingly, many of them flew with electrodynamic tethers (EDTs) [Zhu, 2011]. The primary difference between an EDT and a conventional tether is that the former is electrically conductive and intended to generate an electrical current by the passive electromagnetic interactions with the Earth's magnetic field [Pelaez, 2000]. The induced current interacts with the magnetic field, resulting in a Lorentz force along the EDT length that can affect all aspects of the EDT system dynamics. These missions demonstrated the EDT's potential to provide low-cost orbit transfers, both deorbit and boost without propellant, which is a considerable advantage compared to the conventional tethered satellite systems. In addition, space tether technology has the near term potential to meet a broad range of scientific and engineering demands such as to acquire/generate science data or to provide cost-effective demonstration of innovative concept.

Recently, there are renewed interests on the EDT propulsion technology in NASA [NASA, 2011] and other leading space agencies [Nishid *et al.*, 2009] due to its potential application in space debris mitigation and removal, e.g. the end-of-mission self-deorbit of spacecraft, after the satellite collision between Iridium 33 and Cosmos 2251 in 2009 [Jakhu, 2010]. The EDT propulsion technology is recognized as one of the feasible candidate technologies for space debris removal [Jablonski and Scott, 2009]. Specifically, the EDT technology is the most appealing for the emerging class of micro/nano satellites as more private companies, universities and non-spacefaring nations get access into space via this low-cost platform and left large numbers of obsoleted satellites as debris in space. Unlike the large spacecraft, deorbiting them using a rocket or thruster has a prohibitively high cost or is physically impractical due to the size and/or mass limitation for this class of satellites. Moreover, the EDT technology demonstrated in space by NASA employed an insulated EDT with two hollow plasma contactors at each end. These plasma contactors require consumable fuels to attract and eject electrons from/to ambient ionosphere. Their size and mass do not fit into the micro/nano satellites, nor the required consumables. The alternative to the insulated EDT with hollow plasma contactors is the bare EDT as anode with field effect cold-cathode electrode emitter at its end [Zhu, 2011]. It is particularly appealing to the micro/nano satellites due to its high efficiency in generating current, light mass and compact size.

Although the EDT propulsion technology has been extensively studied and some EDT missions have flown in the past, there is no detailed study of deorbiting nanosatellite using the bare EDT. In addition, most works deal with EDT deorbiting in near equatorial orbits or orbit with low inclination angles. It is widely believed, without detailed analysis, that the spacecraft deorbit by EDT in near polar orbits is inefficient because the electromotive force in the EDT will become minimal in the polar orbit. This has motivated the current study of deorbiting a nano satellite system using a bare EDT for any orbit inclination angles.

2. Dynamics of Electrodynamic Tether Satellite System

2.1. *Orbital equations*

Consider an EDT satellite system that can be simplified as a two-body system consisting of two end masses (m_1 and m_2) connected by a rigid tether of length L and a mass m_t. The upper mass is m_1 and the lower one is m_2. Let us assume a geocentric inertial frame of Earth ($Oxyz$) with the origin at the Earth's center, the x-axis directs to the point of vernal equinox, the z-axis aligns with the rotation axis of Earth, and the y-axis completes the system with a right-hand coordinate system, see Fig. 1. The motion of the system relative to the geocentric inertial frame of Earth can be described by two common forms of orbital equations. The first is the direct description of the system motion in the Cartesian coordinates (x, y, z). For the two-body problem with perturbations, the equation of motion can be written as,

$$\ddot{\vec{\mathbf{r}}} = -\frac{\mu}{|\vec{\mathbf{r}}|^3}\vec{\mathbf{r}} + \vec{\mathbf{F}}, \tag{1}$$

where μ is the gravitational parameter of Earth, $\vec{\mathbf{r}} = \vec{\mathbf{r}}(x, y, z)$ is the position vector, $\vec{\mathbf{F}}$ is the perturbation force vector acting on the EDT satellite system, respectively. Equation (1) is highly nonlinear and is usually solved by the Cowell method [Montenbruck, 1992] numerically. Due to the nonlinearity of Eq. (1), the time integration step size is limited in this method because the Cartesian coordinates change rapidly in orbital motion.

The other form of orbital equations is the Gaussian perturbation equations that describe the orbital motion of the EDT system by six constants called the orbital

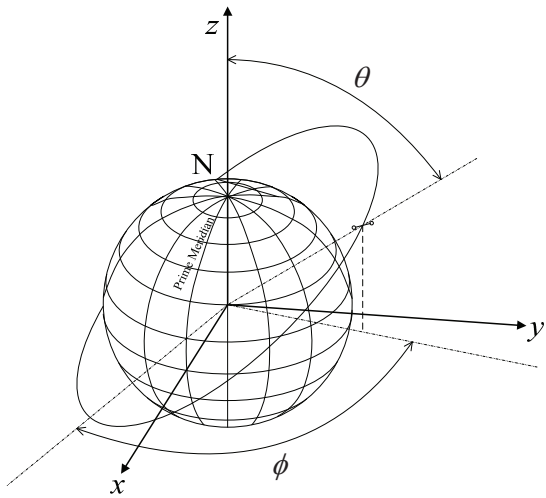

Fig. 1. Illustration of system coordinates.

elements, such as,

$$\frac{d\vartheta_j}{dt} = f(\vartheta_1, \vartheta_2, \vartheta_3, \vartheta_4, \vartheta_5, \vartheta_6, T, S, W), \tag{2}$$

where ϑ_j $(j = 1, 2, \ldots, 6)$ are the orbital elements, T, S, and W are the three orthogonal perturbation force components in an orbital plane coordinate system, respectively. The first two force components are in the orbital plane with T is the radial force component and S is the force component perpendicular to T and pointed in the direction of satellite motion. The third force component W completes a right-hand system. Since 5 out of 6 orbital elements are constant in the case of two-body problem, we adopted the Gaussian perturbation equations in this paper. It has lesser constraints on the numerical integration step size because the orbit elements vary much slower than the Cartesian coordinates, which is beneficial for the calculation of orbital life of the EDT system.

2.2. *Orbital perturbation forces*

There are several perturbation forces acting on an EDT satellite system orbiting around the Earth, namely, (i) the electrodynamic force on a current-carrying EDT, (ii) the Earth's atmospheric drag, (iii) the non-homogeneity and oblateness of Earth, (iv) third-body (Sun and Moon) perturbing forces, (v) solar radiation, and (vi) spacecraft thrust. For the self-deorbit of EDT satellite system in low Earth orbit (LEO) less than 1000 km, the effects of the gravitational perturbation of Sun and Moon and the solar radiation are small and negligible. In addition, the EDT satellite system is assumed thrust-less during the deorbiting process. Therefore, we will consider only the first three perturbation forces in the deorbit dynamic analysis.

2.2.1. *Electrodynamic force*

Assume the EDT is stabilized in the local vertical by the differential gravitational force as shown in Fig. 2 and the libration of EDT is neglected. As the bare conductive EDT crossing the Earth's magnetic field at orbital velocity, an electromotive force E_m will be induced along the EDT length that can be calculated under the formula of Sanmartin [2010],

$$E_m = \frac{dV_p}{ds} = (\vec{\mathbf{v}} \times \vec{\mathbf{B}}) \cdot \vec{\mathbf{l}}, \tag{3}$$

where V_p is the motion induced voltage, s is the local coordinate along EDT length, $\vec{\mathbf{v}}$ is the velocity vector of EDT with respect to the Earth's magnetic field, $\vec{\mathbf{B}}$ is the local magnetic field strength of Earth, and $\vec{\mathbf{l}}$ is the unit vector along the EDT length, respectively. The magnetic field strength of Earth can be described by Legendre

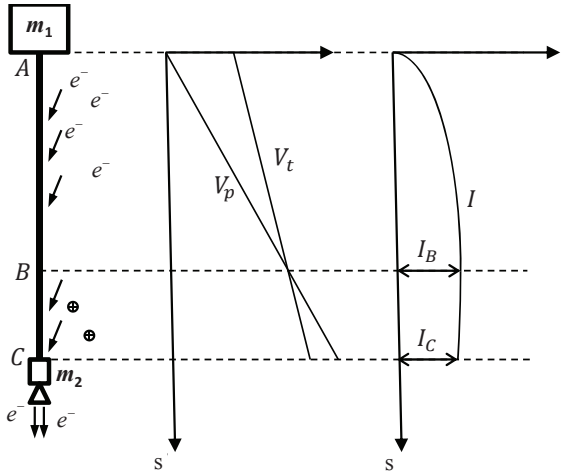

Fig. 2. Scheme of an electrodynamic bare tether and the voltage/current variation. A, C denote anodic and cathodic ends respectively. B is the point where potential bias is equal to zero.

polynomials using IGRF2000 model [Davis, 2004; James, 1978], such that,

$$\tilde{\mathbf{B}} = \begin{Bmatrix} B_r \\ B_\theta \\ B_\phi \end{Bmatrix} = \begin{Bmatrix} \sum_{n=1}^{\infty} \left(\frac{r_0}{r}\right)^{n+2} (n+1) \sum_{m=0}^{n} [g_n^m \cos(m\phi) + h_n^m \sin(m\phi)] P_n^m(\theta) \\ -\sum_{n=1}^{\infty} \left(\frac{r_0}{r}\right)^{n+2} \sum_{m=0}^{n} [g_n^m \cos(m\phi) + h_n^m \sin(m\phi)] \frac{\partial P_n^m(\theta)}{\partial \theta} \\ \frac{-1}{\sin\theta} \sum_{n=1}^{\infty} \left(\frac{r_0}{r}\right)^{n+2} \sum_{m=0}^{n} m[-g_n^m \sin(m\phi) + h_n^m \cos(m\phi)] P_n^m(\theta) \end{Bmatrix} \tag{4}$$

where r_0 is the reference radius of Earth ($r_0 = 6371.2\,\text{km}$), $r = |\vec{\mathbf{r}}|$ is the geocentric radius, θ is the co-latitude ($\theta = 90^\circ - \text{latitude}$), and φ is the longitude. B_r, B_θ, and B_φ are the components of field strength represented in the spherical coordinates (r, θ, φ), respectively. The coefficients g_n^m and h_n^m are Gaussian coefficients put forth by the IAGA for the IGRF, and $P_n^m(\theta)$ represents the Schmidt quasi-normalized associated Legendre functions of degree n and order m. Detailed expressions of these coefficients can be found in [Davis, 2004].

The resulting electromotive force will make it partially positive and partially negative charged relative to the ambient ionospheric plasma depending on difference between the motion induced voltage (V_p) and the EDT voltage due to the ohmic loss (V_t), see Fig. 2. Consequently, the electrons in the ionosphere will be collected by the positive biased bare EDT while the ions will be collected by the negative biased part of EDT [Kruijff *et al.*, 2009], resulting a current across in the EDT if there is an electron and ion emitting device at the each ends of EDT to expel the

electrons and ions back into the ionosphere to complete the current loop, as shown in Fig. 2. Accordingly, the induced current can be described as [Sanmartin, 1993; Sanjurjo-Rivo, 2009]

$$\frac{dI}{ds} = en_\infty d \begin{cases} (2e\Delta V/m_e)^{1/2} & \text{if } V_t > V_p, \\ -(-2e\Delta V/m_i)^{1/2} & \text{if } V_t < V_p, \end{cases} \tag{5}$$

where $\Delta V = V_t - V_p$, I is the induced current, e is the electron charge, n_∞ is the unperturbed plasma density, d is the tether diameter, m_e and m_i are the mass of electron and ion, respectively.

The EDT potential varies due to ohmic loss, depending on the current flow I. Therefore, the relationship between the potential bias and the current can be written as,

$$\frac{d\Delta V}{ds} = \frac{I}{\sigma A} - E_m, \tag{6}$$

where σ is the conductivity of EDT and A is the cross section area of tether.

Equations (5) and (6) form the base of EDT voltage-current relationship. Generally, the numbers of ions collected are much fewer than electrons and can be neglected because the mass of ion is much greater than electron. Therefore, we can assume the current is constant ($dI/ds \approx 0$) in the tether segment $\overline{BC}$ where $\Delta V < 0$. The induced current in the EDT will interact with the magnetic field of Earth to generate the Lorentz force on the EDT, such that,

$$d\vec{\mathbf{F}}_\mathbf{B} = -\vec{\mathbf{B}} \times I(s)\vec{\mathbf{l}}\, ds. \tag{7}$$

Correspondingly, the power dissipated by the EDT is,

$$P = \int_0^L \vec{\mathbf{v}} \cdot d\vec{\mathbf{F}}_\mathbf{B} = -\int_0^L \vec{\mathbf{v}} \cdot (\vec{\mathbf{B}} \times \vec{\mathbf{l}}) I(s) ds = -\int_0^L (\vec{\mathbf{v}} \times \vec{\mathbf{B}}) \cdot \vec{\mathbf{l}}\, I(s) ds, \tag{8}$$

where L is the length of tether.

Substituting Eqs. (3) and (6) into Eq. (8) leads to

$$P = -\int_0^L E_m I(s) ds \le -\int_0^L \frac{\sigma A}{2} \left(\frac{I^2}{(\sigma A)^2} + E_m^2 \right) ds \le 0. \tag{9}$$

Equation (9) indicates that the power dissipated by the EDT motion is always negative, which indicates the induced Lorentz force is always against the motion of EDT even in the case of polar orbit where the induced current in the EDT can reverse its direction as the EDT moves from the north pole to the south pole. This is the principle of deorbiting spacecraft by EDT — using the electrodynamic force as drag.

2.2.2. *Aerodynamic force*

The aerodynamic force on the EDT is resulted from the atmosphere drag if the tangential component is ignored, such that,

$$d\vec{\mathbf{F}}_A = \frac{1}{2}\rho C_d d|\vec{\mathbf{v}}_\mathbf{r}|\vec{\mathbf{v}}_\mathbf{r} ds, \tag{10}$$

where ρ is the air density, C_d is the drag coefficient, d is the EDT diameter, and $\vec{\mathbf{v}}_\mathbf{r}$ is the relative air velocity with respect to the EDT, respectively. Assuming the atmosphere rotates with the Earth in the same rate, the relative air velocity can be determined as,

$$\vec{\mathbf{v}}_\mathbf{r} = \vec{\mathbf{v}} - \vec{\boldsymbol{\omega}} \times \vec{\mathbf{r}}, \tag{11}$$

where $\vec{\boldsymbol{\omega}}$ is the Earth's self-rotational rate and $\vec{\mathbf{r}}$ is the position of EDT in the geocentric inertial frame of Earth.

The drag coefficient C_d in free-molecular hyperthermal flow in space depends on the momentum exchange that occurs between the molecules and arresting surface of spacecraft, which are generally considered to be functions of surface materials of that spacecraft. For a circular cylinder in hyperthermal flow, the normal drag coefficient is almost constant at $C_d = 2.2$ [Storch, 2002]. However, the density of air varies rapidly over the altitude. We adopted the atmosphere model of U.S. Standard Atmosphere [Lewis, 2007] in this paper, which provided valid data of atmosphere parameters such as temperature, pressure, and density at desired altitudes between sea level and 1000 km. As a comparison, we also investigated the empirical model by Carroll [1997], which is much simple and easier to implement,

$$\rho \approx \frac{1.47 \times 10^{-16} T_{ex}(3000 - T)}{[1 + 2.9(H - 200)/T]^{10}}, \quad H > 200\,\text{km}, \tag{12}$$

where T is the temperature in Kelvin and H is the altitude in kilometers. The best estimation is 0.5ρ $(T = 1100K)$. The comparison between the Standard Atmosphere 1976 and the best estimation is shown in Fig. 3, where the dashed line denotes the Standard Atmosphere 1976 and the solid line denotes the empirical model in Eq. (12).

Obviously, these two models matched quite well when the height is between 200 km and 800 km. The air density calculated using the empirical formula is much conservative above 800 km for orbit life time calculation.

2.2.3. *J2 perturbation force due to oblateness of earth*

The geoid is roughly an oblate ellipsoid. As a result, the satellite orbiting Earth is attracted not only to its center but also towards its equator. The latter imposes a torque on a satellite in any orbit planes that across the equator at an angle, resulting in the direction of the orbital angular momentum vector to regress. The

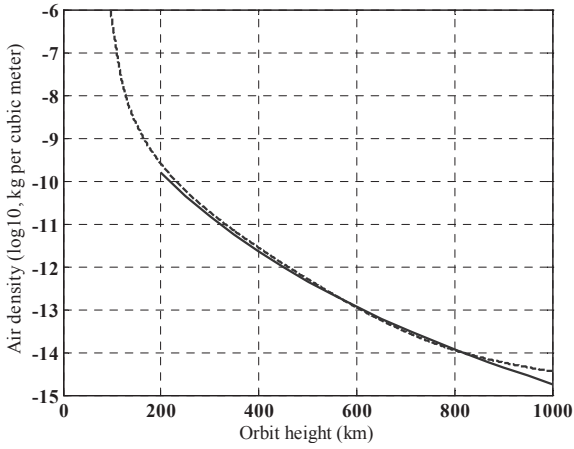

Fig. 3. Comparison of atmospheric models.

daily increase of the ascending node caused by J_2 perturbation, which is the major term of oblateness perturbation, is described as followed [Curtis, 1988]

$$\Delta\Omega = -9.97\left(\frac{r_0}{a}\right)^{7/2}\cos i_o, \tag{13}$$

where a is the semi-major axis of the orbit and i_o is the orbital inclination angle. In this paper, we will examine the impact of this effect on the deorbiting rate of a tethered satellite system.

3. Simplification and Numerical Procedure

It has been shown in Sec. 2 that the governing equations of EDT dynamics are highly nonlinear. For later convenience, we introduce three dimensionless variables, such that,

$$\varepsilon = s/L_0; \quad i = I(s)/I_0; \quad \lambda = \Delta V/V_0, \tag{13}$$

where L_0, I_0 and V_0 are defined as the unit length, current, and voltage as follows:

$$L_0 = \left(\frac{9\pi m_e \sigma^2 E_m A}{128 e^2 n_\infty^2}\right)^{1/3}; \quad I_0 = \sigma E_m A; \quad V_0 = E_m L_0. \tag{14}$$

Note that the I_0 is also called the short circuit current in the literature.

Substituting Eqs. (13) and (14) into Eqs. (5) and (6) leads to dimensionless equations for the voltage-current relationship, such that,

$$\frac{di}{d\varepsilon} = \frac{3}{4}\sqrt{\lambda}, \tag{15}$$

$$\frac{d\lambda}{d\varepsilon} = i - 1, \tag{16}$$

which are subjected to boundary conditions:

$$\varepsilon = 0: \quad i = 0, \quad \lambda = \lambda_A$$

$$\varepsilon = \varepsilon_B: \quad i = i_B = i_C, \quad \lambda = 0.$$

Integrating Eqs. (15) and (16) with the given boundary conditions results in the following solutions,

$$\lambda_A = (2i_C - i_C^2)^{2/3}, \tag{17}$$

$$\varepsilon_B = \int_0^{\lambda_A} (\lambda^{3/2} - \lambda_A^{3/2} + 1) d\lambda. \tag{18}$$

However, the integration of Eq. (18) depends on the maximum current generated by EDT that in turn depends on the positive biased length of tether segment $\overline{AB}$. Unfortunately, the length of this segment is unknown and additional boundary condition is required. This boundary condition is usually determined by mission objectives and electron emitting devices at the end of EDT. Here, we consider two types of boundary conditions:

(1) *Assume i_c is known*

In the electron emitting device is determined, the current at cathode end is often chosen as a design parameter. Then, the positive biased tether length and the potential bias at anode end can be calculated directly from Eqs. (17) and (18). Accordingly, Eqs. (15) and (16) can be integrated.

(2) *Assume the whole tether is positive biased*

In this situation, the parameter ε_B is a known constant. This boundary condition is used to investigate the maximum deorbiting capacity of EDT (named as full power tether hereafter), and it is more complicated to deal with compared with the previous boundary condition. Optimization algorithms are required to solve λ_A from Eq. (18) that provides an initial condition for the integration.

Unfortunately, the integration of the voltage-current relationship must be repeated at every time step in simulating the deorbiting process of EDT because the environment is changing all the times. Thus, a life-time simulation of a deorbiting EDT initially from an orbit with high altitude will be time consuming. To reduce the computational effort, some works [Sanmartin, 2010] bypassed the integration of the voltage-current equations by using the short circuit current as an approximation. However, this approach will overestimate the electrodynamic force because the short circuit current is difficult to obtain for a near polar or higher-altitude orbit where the electromotive force $\vec{\mathbf{v}} \times \vec{\mathbf{B}}$ is weak or a short bare EDT where there is not sufficient length of EDT as anode to attract electrons from ambient ionosphere.

Hereafter, we derive a simplified yet effective analytical method to integrate the voltage-current equations.

Assume the dimensionless current (ratio to the short circuit current) is very small, i.e., $i \ll 1$, either due to the weak electromotive force $\vec{\mathbf{v}} \times \vec{\mathbf{B}}$ or short tether, Eq. (16) yields

$$\frac{d\lambda}{d\varepsilon} = -1. \tag{19}$$

Integration of Eq. (19) gives

$$\lambda = \lambda_A - \varepsilon. \tag{20}$$

Substituting Eq. (20) into Eq. (15) yields

$$\frac{di}{d\varepsilon} = \frac{3}{4}\sqrt{\lambda_A - \varepsilon}. \tag{21}$$

Then, the current can be solved by integration of Eq. (21) as

$$i = \frac{1}{2}\lambda_A^{3/2} - \frac{1}{2}(\lambda_A - \varepsilon)^{3/2}. \tag{22}$$

Therefore, the average current density across the tether that generates the same Lorentz force should be

$$i_{avg} = \frac{1}{L}\left[\int_0^{\varepsilon_B} i d\varepsilon + i_C(L - \varepsilon_B)\right] = -\frac{1}{5L}\lambda_A^{5/2} + \frac{1}{2}\lambda_A^{3/2} \tag{23}$$

Equation (23) gives an analytical expression for the current and it can be used in the Lorentz force calculation for the near polar orbit or short EDT in order to improve the computational efficiency significantly.

4. Simulation Results

4.1. *System parameters*

Parameters used in this paper are coming from a mission concept proposed for engineering and scientific applications using nanosatellite formation flying with electrodynamic tether [Zhu, 2011]. The simulation results can be used for advanced mission study. Values of major parameters are listed in Table 1. For the sake of simplicity, the plasma density n_∞ is assumed to be a constant of $10^{11}\,m^{-3}$.

4.2. *Deorbit of tethered satellite system by air drag only*

To investigate the efficiency of EDT propulsion in deorbiting a satellite system, we first establish a deorbiting baseline by considering the air drag only. It is assumed that the EDT satellite system initially runs in a circular orbit with orbit height of 1000 km, and the targeted altitude is 250 km. In addition to the air drag, we also investigate the impact of the Earth's oblateness and the inclination angle of orbit on the orbit-life of the EDT satellite system together with the air drag.

Table 1. Parameters of an EDT satellite system [Zhu, 2011].

Parameters	Values
Mass of Primary Satellite	5 kg
Mass of Secondary Satellite	1.75 kg
Mass of Tether	0.25 kg
Dimensions of Primary Satellite	$0.02 \times 0.02 \times 0.02$ m
Dimensions of Secondary Satellite	$0.01 \times 0.017 \times 0.01$ m
Tether Length	500 m
Tether Diameter	0.5 mm
Tether Conductivity (aluminum)	$3.4014 \times 10^7 \Omega^{-1}\text{m}^{-1}$
Drag Coefficients	Tether – 2.2, and End Satellites – 1.6
Orbit Altitudes	250∼1000 km
Orbit Inclination	0∼90 degrees

Figure 4 shows the deorbiting result of the EDT satellite system initially running in a polar orbit with and without Earth oblateness perturbation (J2, J3, and J4 effect included). It is found that the oblateness perturbation does affect the orbit eccentricity, causing the altitude oscillating with the orbit frequency. However, the total time of orbit-life is not affected much. There exists a short period effect in oblateness perturbation, which limits the integration step size of orbital equations. Therefore, this perturbation can be ignored in orbit-life estimation for simplicity and computational efficiency.

Next, Fig. 5 gives the relationship between the orbit descending rate and the orbit inclination angle with the detailed information is shown in Fig. 6 for the first 100 km reduction of orbit altitude. It is shown in the figures that the total time of orbit life increases when the inclination angle of the orbit decreases. The reason is that the magnitude of relative air velocity reduces as the inclination angle decreases, see Eq. (11). The effect is quite significant at high altitude and diminishes as the orbit altitude reduces below 700 km.

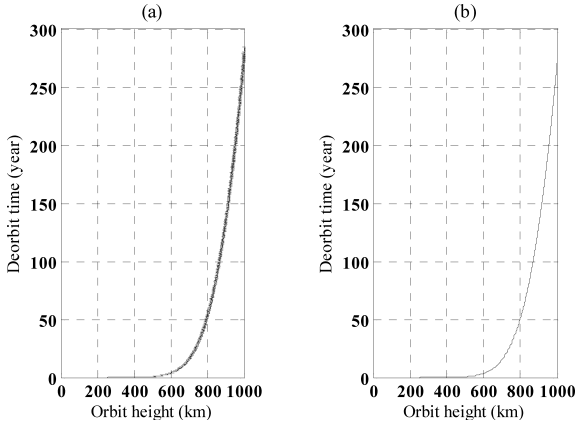

Fig. 4. EDT satellite system descending rate with air drag only: (a) with oblateness perturbation (b) without oblateness perturbation.

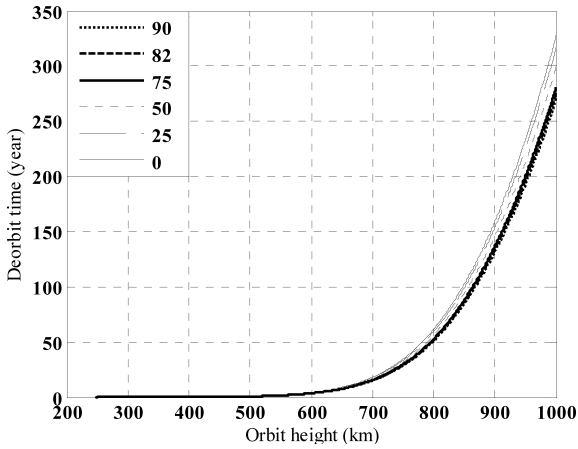

Fig. 5. EDT satellite system descending rate with respect to inclination angle.

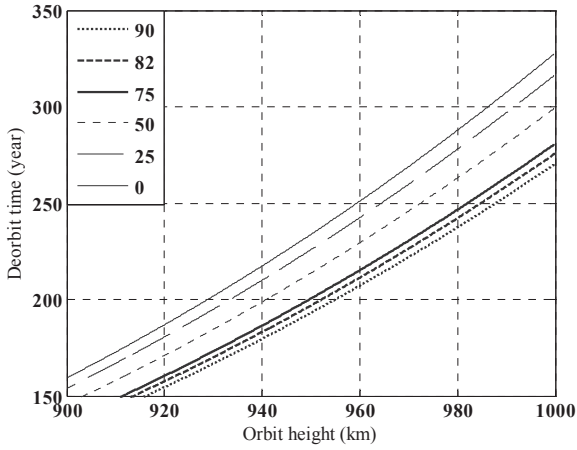

Fig. 6. EDT satellite system descending rate with respect to inclination angle (detailed).

In all cases, the decaying time is very long (>200 years), which is unacceptable for the space debris mitigation. The decaying rate is especially small when the orbit altitude is above 700 km. It indicates that it is required to take the deorbiting means to reduce the orbit life to less than 25 years as required [Jablonski and Scott, 2009].

4.3. *Voltage induced by orbital motion of EDT*

The EDT induced voltage is critical for the deorbiting rate. The motion induced electromotive force E_m depends on the orbit inclination angle and the local strength of the Earth's magnetic field. Most existing works [Sanmartin, 2010] analyzed the electrodynamic behaviors of EDT at low inclination angles and there are only qualitative

statements about the EDT behaviors in polar orbit or orbits with high inclination angles. Moreover, most existing works adopted the first-order approximation of Earth's magnetic field in Eq. (4), which ignores the non-uniformity of Earth's magnetic field and results in inaccurate prediction of the induced voltage as well as the Lorentz force. In this section, we investigated the impact of EDT orbit inclination angles and altitudes on the induced voltage. To include the non-uniform effect of Earth's magnetic field, we adopted six order terms in the calculation of local strength of Earth's magnetic field. For the sake of simplicity, the tether dynamics is ignored in these cases and the tether is assumed to always align with the radius direction.

Simulations of 24 hour period of a descending EDT were carried out on orbit with different orbit inclination angles and altitudes to investigate the induced voltage variation in different situations. The magnetic field strength and orbit velocity along the tether are treated as constant because of the short length. The simulation results are shown in Figs. 7–9.

It is shown in Fig. 7 that the magnitude of induced voltage increases as the inclination angle decreases. This is reasonable because for a polar orbit, the directions of velocity and local magnetic field are almost collinear. The contribution of magnetic field to the induced voltage is only the component along the latitude direction, which is rather small. For orbits with higher inclination angle, the induced voltage will reverse its direction. This is caused by the inclination of Earth's magnetic axis relative to the Earth's self-rotation axis. Therefore, the EDT system in higher inclination orbits is required to have electron emitter at both ends of the tether to work all the time. Otherwise, it works in the most of time during orbit moving until the induced voltage reverses its direction. The phenomenon of voltage/current

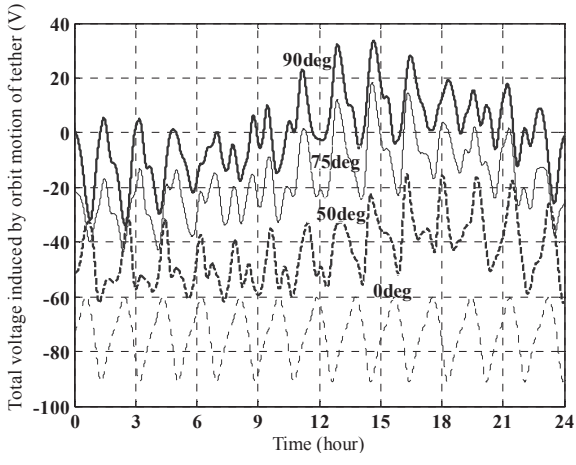

Fig. 7. Induced voltage variations with respect to orbit inclination angle (orbit altitude equal to 1000 km).

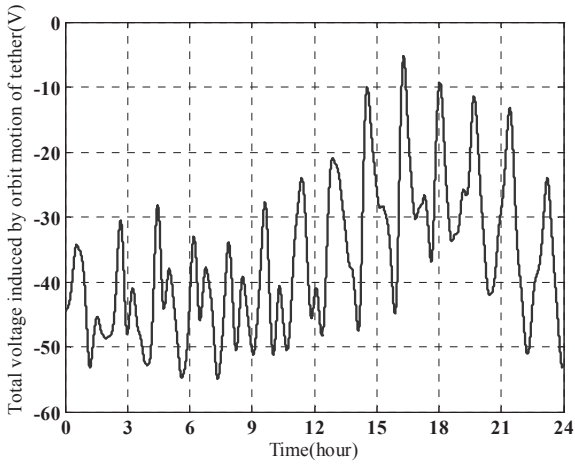

Fig. 8. Induced voltage variation on orbit with inclination of 57 degrees (orbit altitude: 1000 km).

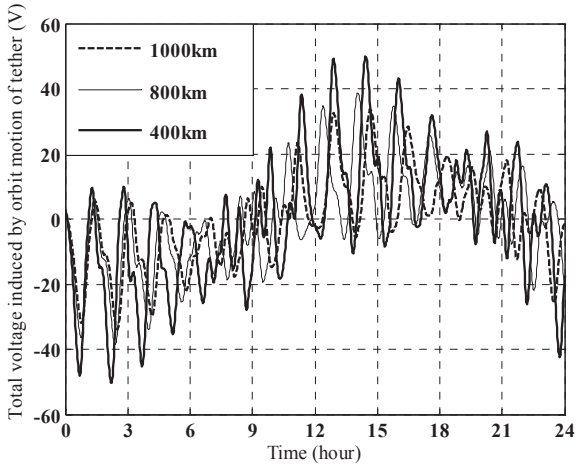

Fig. 9. Induced EDT voltage variation with respect to the orbit altitude in one day (orbit inclination: 90 degrees).

direction change disappears as inclination angle decrease to certain extent where the major contribution of the magnetic field becomes the component along the longitude direction and the influence of the inclination of magnetic axis is small. The critical inclination is about 57 degrees as shown in Fig. 8.

The magnitude of induce voltage increases as orbit altitude decreases due to the stronger magnetic field strength at the low altitude as shown in Fig. 9. This in turn increases the magnitude of the Lorentz force during the deorbiting process and, therefore, accelerates the deorbiting rate.

4.4. *Deorbit of EDT satellite system with electrodynamics force*

This section presents the simulation results of deorbiting EDT Satellite System under both aerodynamic drag and electrodynamic force. As in Fig. 7, the induced voltage over the EDT will reverse its direction if the orbit inclination angle exceeds 57 degrees. Correspondingly, the current in the EDT will reverse its direction and the direction of the Lorentz force will change too. However, this does not limit the usage of EDT on such orbits because the power of the Lorentz force is always negative as proved by Eq. (9), which indicates that the Lorentz force always against the motion of EDT and dissipates the power into heat despite the current in the EDT reverses its direction. Figure 10 plots the time history of power over 24 hours in a polar orbit. It shows the EDT always transforms its mechanical energy into electric energy.

Next, the full power EDT deorbiting processes with different inclination angles are shown in Figs. 11–14. It is found in these figures that the total deorbiting time is reduced significantly comparing with results under air drag only in Fig. 4, which is more obvious when the altitude is over 700km. Deorbiting by EDT works much better for orbits with small inclination angles, because the induced voltage is much larger as shown in Fig. 7. However, the deorbiting time by EDT with large inclination angle is also acceptable (< 25 years). In addition, the simulation results reveal a new finding that has not been noticed before. Although the EDT satellite system starts with a circular orbit, its orbit gradually changes into an elliptical orbit due to non-uniform magnetic field. The eccentricity of the orbit increases as the orbit altitude decrease due to the increase of local strength of the magnetic field. As the orbit altitude further decreases, the effect of air drag starts to exceed the electrodynamic force, leading to the decrease of the orbit eccentricity. In these orbits, the influence of magnetic axis inclination is significant and the eccentricity varies

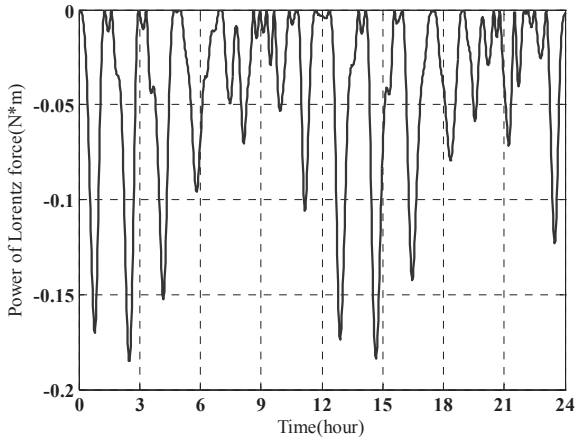

Fig. 10. Variation of power of the Lorentz force of a full power EDT (orbit altitude: 1000 km).

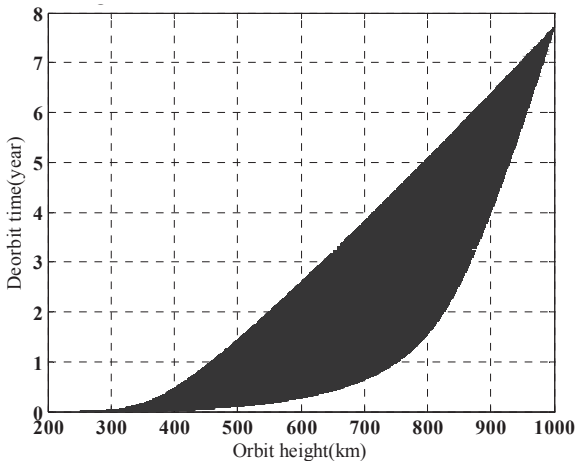

Fig. 11. Deorbiting rate of EDT with initial inclination angle of 90 degrees.

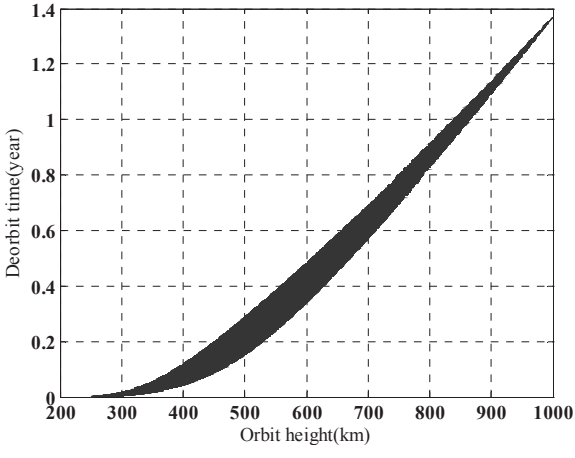

Fig. 12. Deorbiting rate of EDT with initial inclination angle of 60 degrees.

larger than those with small inclination angles due to the periodical perturbation. The large eccentricity is considered beneficial to the deorbiting process of near polar orbits using EDT propulsion technology because with a lower perigee, atmosphere with larger density provides more air drag to dissipate the orbit kinetic energy of satellites faster. This is especially important for polar orbit where the electromotive force is minimal. This phenomenon reduces to the minimum in the equatorial orbit. The reason that it has never been reported before is that (i) most of the existing works adopted the first order approximation of Earth's magnetic field and (ii) the existing works focuses on the equatorial orbit or orbit with small inclination angles where this phenomenon is not significant.

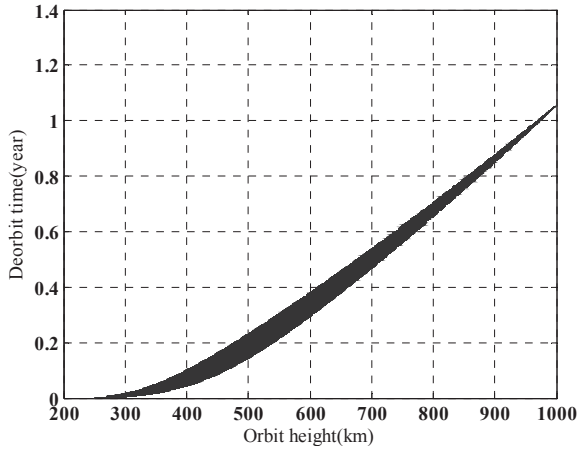

Fig. 13. Deorbiting rate of EDT with initial inclination angle of 30 degrees.

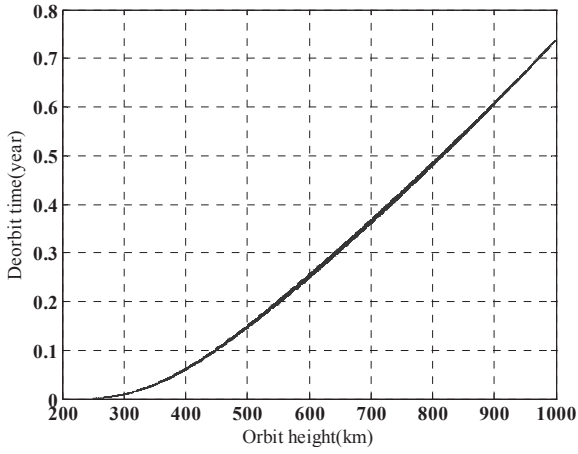

Fig. 14. Deorbiting rate of EDT with initial inclination angle of 0 degrees.

Finally, the result of a partial power EDT is shown in Fig. 15, using 0.015 as the operating dimensionless current at the cathode end. Result of approximate method developed in this paper is also provided as a comparison. It can be found that the deorbiting time predicted by the approximate method is almost the same as that of the accurate model, with the maximal difference less than 0.04 year. The conclusion is obtained that the full power tether decays more quickly than partial power tether after comparing with Fig. 11. However, the difference is not much for a mission using short EDT running on the orbit with large inclination angles. Therefore, the approximate method proposed can be treated as a good estimate for the deorbiting rate in these missions if an appropriate dimensionless current is given.

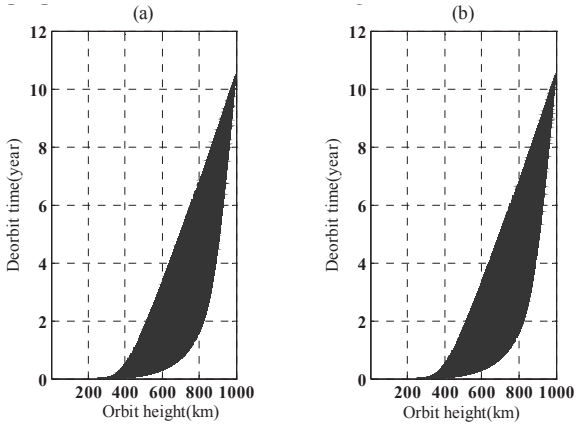

Fig. 15. Deorbiting rate of a partial power EDT with initial inclination angle of 90 degrees. (a) results of accurate model and (b) Results of approximate method.

5. Conclusions

This paper investigated the satellite self-deorbit using the propellantless EDT propulsion technology. Orbital dynamics including environmental perturbations and motion relative electrodynamic model are studied in details. In order to reduce computational efforts in orbit life time calculation, a simplified analytical method is proposed for the prediction of deorbiting rate of an EDT satellite system with small dimensionless current such as missions with a short tether length or large inclination angles. The simulation results show that the proposed simplified analytical method is accurate and computational efficient in comparison with the accurate model. The analyses also indicated that the induced electromotive force reverses its direction across the EDT in the polar orbit or orbits with higher inclination angles, causing the current reverses its direction in the EDT and the current induced Lorentz force changes its direction. However, the power of the Lorentz force remains negative in that process, which indicates the passive EDT always dissipates orbital kinetic energy to lower the altitude of orbit in all orbits.

Furthermore, the simulation results reveal that the orbit of an EDT satellite system will become elliptical in the deorbiting process due to the higher order perturbation of Earth's magnetic field, which has not been reported before due to the grossly oversimplified model of Earth's magnetic field. The orbital eccentricity reaches the maximum in the polar orbit and the minimum in the equatorial orbit. This is specifically beneficial to deorbit a satellite orbiting in the polar orbit or orbits with higher inclination angles where the electrodynamic force is less effective, because the atmosphere with larger density at a lower perigee provides more air drag to dissipate the orbital kinetic energy of the satellite faster. Simulation results show that the orbit life time will be reduced by orders of magnitude with the EDT propulsion compared with the air drag only in all orbits. They demonstrate the EDT propulsion technology can be used in near polar orbits for deorbiting a satellite.

Acknowledgments

This work is supported by the Discovery Grant of Natural Sciences and Engineering Research Council of Canada.

References

Bombardelli, C., Lorenzini, E. C. and Quadrelli, M. B. [2004] "Retargeting dynamics of a linear tethered interferometer," *Journal of Guidance, Control, and Dynamics* **27**(6), 1061–1067.

Carroll, J. [1993] "SEDS deployer design and flight performance," *Proceeding of AIAA Space Programs and Technologies Conference and Exhibit 21–23*, Huntsville, United States.

Carroll, J. A. [1997] "Guidebook for analysis of tether applications," in *Tethers in Space Handbook*, 3rd ed., eds. M. L. Cosmo, and E. C. Lorenzini (NASA Contract Rep. NASA-CR-97-206807), pp. 152–186.

Cartmell, M. P. and McKenzie, D. J. [2008] "A review of space tether research," *Progress in Aerospace Sciences* **44**(1), 1–21.

Curtis, H.D. [1988] *Orbital Mechanics for Engineering Students* (Elsevier Butterworth-Heinemann, Oxford).

Davis J. [2004] "Mathematical modeling of Earth's magnetic field," Technical Note, Virginia Tech., Blacksburg.

Fujii H. [2010] "Tether technology for space solar power satellite and space elevator," *Procedings of 61th International Astronautical Congress of the International* Astronautics *Federation*, Prague, Czech Repulic, IAC Paper 10–D4.3.3

Hoyt R., Slostad J. and Mazzoleni A. P. [2003] "The multi-application survivable tether (MAST) experiment," *Proc. of the 39th AIAA/ASME/SAE/ASEE Joint Propulsion Conference and Exhibit* 20–23, Huntsville, United States.

Jablonski, A. M. and Scott R. [2009] "Deorbiting of microsatellites in Low Earth Orbit (LEO) — An *Introduction*," *Can. Aeronaut Space Journal* **55**(2), 55–67.

Jakhu R. S. [2010] "Iridium-Cosmos collision and its implications for space operations" in *ESPI Yearbook on Space Policy. 2008/2009: Setting New Trends* (Wien Springer, New York), pp. 254–275

James, R. W. [1978] *Spacecraft Attitude Determination and Control* (D. Reidel Publishing Company, Boston, MA).

Kruijff, M., van der Heide, E. J. and Ockels, W. J. [2009] "Data analysis of a tethered SpaceMail experiment," *Journal of Spacecraft and Rockets* **46**(6), 1272–1287.

Kumar, K. D. [2006] "Review of dynamics and control of nonelectrodynamic tethered satellite systems," *Journal of Spacecraft and Rockets* **43**(4), 705–720.

Lewis, B. [2007] "Complete 1976 Standard Atmosphere," http://www.mathworks.com/matlabcentral/fileexchange/13635-complete-1976-standard-atmosphere (accessed Aug. 2011).

Montenbruck, O. [1992] "Numerical integration methods for orbital motion," *Celestial Mechanics and Dynamical Astronomy* **53**(1), 59–69.

NASA MSFC RFI: "Electrodynamic tether propulsion demonstration mission," Available online at: http://www.spaceref.com/news/viewsr.rss.html?pid=34809 (accessed Feb. 2011)

Nishid, S. I. *et al.* [2009] "Space Debris Removal System Using a Small Satellite," *Acta Astronautica* **65**(1–2), 95–102.

Pardini, C., Hanada, T. and Krisko, P. H. [2009] "Benefits and risks of using electrodynamic tethers to deorbit spacecraft," *Acta Astronautica* **64**(5–6), 571–588.

Pelaez, J. *et al.* [2000] "A new kind of dynamic instability in electrodynamic tethers," *Journal of Astronautical Sciences* **48**(4), 449–476.

Sanjurjo-Rivo, M. [2009] "Self-balanced bare electrodynamic tethers. Space Debris Mitigation and other Applications," PhD thesis, Applied Physics Aerospace Engineering Department Universidad Politécnica de Madrid, Madrid, Spain.

Sanmartin, J. R., Martinez-Sanchez, M. and Ahedo E. [1993] "Bare wire anodes for electordynamic tethers," *Journal of Propulsion and Power* **9**(3), 353–360.

Sanmartin, J. R. [2010] "A review of electrodynamic tethers for science applications," *Plasma Source Science and Technology* **19**(3), 34022–34028.

Storch, J. A. [2002] *Aerodynamic Disturbances On Spacecraft In Free-Molecular Flow* (AEROSPACE REPORT NO. TR-2003(3397)-1, The Aerospace Corporation, El Segundo, CA)

Wen, H., Jin, D. Hu, H. [2008] "Advances in dynamics and control of tethered satellite systems," *Acta Mech Sin* **24**(3), 229–241.

Zhu, Z. H. [2011] "Mission concept of electrodynamic tether flying for propellantless propulsion demonstration and radio science experiment," *CSME Bulletin* (Spring 2011), pp. 20–27.